Growth, strain relaxation properties and high- dielectric integration of mixed-anion GaAs1-ySby metamorphic materials

Y. Zhu, M. Clavel, P. Goley, and M. K. Hudait

Citation: Journal of Applied Physics **116**, 134304 (2014); doi: 10.1063/1.4896880
View online: http://dx.doi.org/10.1063/1.4896880
View Table of Contents: http://scitation.aip.org/content/aip/journal/jap/116/13?ver=pdfcov
Published by the AIP Publishing

Growth, strain relaxation properties and high-κ dielectric integration of mixed-anion $GaAs_{1-y}Sb_y$ metamorphic materials

Y. Zhu, M. Clavel, P. Goley, and M. K. Hudait[a)]
Advanced Devices & Sustainable Energy Laboratory (ADSEL), Bradley Department of Electrical and Computer Engineering, Virginia Tech, Blacksburg, Virginia 24061, USA

(Received 25 June 2014; accepted 18 September 2014; published online 1 October 2014)

Mixed-anion, $GaAs_{1-y}Sb_y$ metamorphic materials with a wide range of antimony (Sb) compositions extending from 15% to 62%, were grown by solid source molecular beam epitaxy (MBE) on GaAs substrates. The impact of different growth parameters on the Sb composition in $GaAs_{1-y}Sb_y$ materials was systemically investigated. The Sb composition was well-controlled by carefully optimizing the As/Ga ratio, the Sb/Ga ratio, and the substrate temperature during the MBE growth process. High-resolution x-ray diffraction demonstrated a quasi-complete strain relaxation within each composition of $GaAs_{1-y}Sb_y$. Atomic force microscopy exhibited smooth surface morphologies across the wide range of Sb compositions in the $GaAs_{1-y}Sb_y$ structures. Selected high-κ dielectric materials, Al_2O_3, HfO_2, and Ta_2O_5 were deposited using atomic layer deposition on the $GaAs_{0.38}Sb_{0.62}$ material, and their respective band alignment properties were investigated by x-ray photoelectron spectroscopy (XPS). Detailed XPS analysis revealed a valence band offset of >2 eV for all three dielectric materials on $GaAs_{0.38}Sb_{0.62}$, indicating the potential of utilizing these dielectrics on $GaAs_{0.38}Sb_{0.62}$ for p-type metal-oxide-semiconductor (MOS) applications. Moreover, both Al_2O_3 and HfO_2 showed a conduction band offset of >2 eV on $GaAs_{0.38}Sb_{0.62}$, suggesting these two dielectrics can also be used for n-type MOS applications. The well-controlled Sb composition in several $GaAs_{1-y}Sb_y$ material systems and the detailed band alignment analysis of multiple high-κ dielectric materials on a fixed Sb composition, $GaAs_{0.38}Sb_{0.62}$, provides a pathway to utilize $GaAs_{1-y}Sb_y$ materials in future microelectronic and optoelectronic applications. © *2014 AIP Publishing LLC*. [http://dx.doi.org/10.1063/1.4896880]

I. INTRODUCTION

$GaAs_{1-y}Sb_y$ is a promising material currently being considered for both microelectronic and optoelectronic applications. The use of $GaAs_{1-y}Sb_y$ as an active layer material has been reported for high performance tunnel field effect transistors (TFETs),[1–4] ultra-low noise high electron mobility transistors,[5] and near infrared photodetectors.[6] Moreover, $GaAs_{1-y}Sb_y$ can also be used as a metamorphic buffer to provide a high-quality "virtual" substrate for integrating high-performance devices with flexible substrates.[7–9] Utilization of GaAsSb for multi-functional device applications demands high-quality $GaAs_{1-y}Sb_y$ with various antimony (Sb) alloy compositions. Thermodynamic theory predicts that a miscibility gap exists for $GaAs_{1-y}Sb_y$ alloys having Sb compositions in between 25% and 70%,[10–12] which would lead to spinodal decomposition of the $GaAs_{1-y}Sb_y$ material. The spinodal decomposition is expected to be suppressed to a large extent using thermodynamically non-equilibrium growth techniques,[10] such as molecular beam epitaxy (MBE). However, the MBE growth of mixed-anion (III-V-V') alloys poses an increased challenge in precisely controlling the alloy composition, as compared with the MBE growth of mixed-cation (III-III'-V) counterparts, owing to the strong competition between differing incorporation rates among anions due to their dissimilar sticking coefficients.[5,6,13] Unlike mixed-cation ternary alloys, in which the alloy composition is determined by the flux ratios of the group-III elements over a wide range of temperatures, the composition of mixed-anion ternary alloys also depends on the growth temperature.[5,6,13] Moreover, it has been reported that the As/Sb ratio[6] and Ga flux[6] can also influence the Sb alloy composition in $GaAs_{1-y}Sb_y$ material during MBE growth, which adds further complexity in controlling Sb compositions. As a result, it is of critical importance to study in detail the impact of different growth parameters, such as Sb/Ga ratio, As/Ga ratio, and substrate temperature, on Sb composition in $GaAs_{1-y}Sb_y$ materials during the MBE growth process. In addition, proper high-κ dielectric materials with acceptably low interface trap densities and high band offset values between the high-κ dielectric material and the GaAsSb layer are necessary in order to utilize $GaAs_{1-y}Sb_y$ as an active layer material for low-power logic applications.[14] Recent efforts have focused on the investigation of high-κ dielectrics on either III-As[15–17] or III-Sb[18–20] materials, whereas the study of different high-κ dielectrics on mixed As/Sb based materials has not been addressed. In practice, for low-power logic applications a high Sb composition (>60%) is desired in $GaAs_{1-y}Sb_y$ active layers in order to fully utilize the advantage of a lowered bandgap energy and a reduced effective mass.[1,2] In this respect, the selection of suitable high-κ dielectrics with sufficient conduction and valence band offsets (>1 eV) on high Sb composition in $GaAs_{1-y}Sb_y$ materials is essential in minimizing carrier injection from the semiconductor into the high-κ material.[21]

[a)]Telephone: (540) 231-6663. Fax: (540) 231-3362. E-mail: mantu.hudait@vt.edu

In this paper, mixed-anion $GaAs_{1-y}Sb_y$ materials with a wide range of Sb compositions from 15% to 62% were grown by solid source MBE on GaAs substrates. The influence of growth parameters, such as Sb/Ga ratio, As/Ga ratio, and substrate temperature, on the Sb composition of $GaAs_{1-y}Sb_y$ was systemically investigated. The strain relaxation properties of MBE grown $GaAs_{1-y}Sb_y$ materials with various Sb compositions were studied using high-resolution x-ray diffraction (XRD). Three different high-κ dielectrics, Al_2O_3, HfO_2, and Ta_2O_5, were integrated on $GaAs_{0.38}Sb_{0.62}$ utilizing atomic layer deposition (ALD). The band alignments of these high-κ dielectrics on $GaAs_{0.38}Sb_{0.62}$ were investigated by x-ray photoelectron spectroscopy (XPS). The comprehensive investigation of Sb/Ga ratio, As/Ga ratio and substrate temperature influence on Sb composition during MBE growth, coupled with a quantification of the band structures at several high-κ dielectric/$GaAs_{0.38}Sb_{0.62}$ heterointerfaces, will facilitate the utilization of $GaAs_{1-y}Sb_y$ materials in future microelectronic and optoelectronic applications.

II. EXPERIMENTAL

All $GaAs_{1-y}Sb_y$ structures were grown by Veeco modified Gen-II solid source MBE on semi-insulating GaAs (001) substrates. The Sb flux was provided by an Sb effusion cell. A valve cracker was used to provide the arsenic (As) flux with the cracking zone held at 900 °C to ensure a consistent As_2 flux during the growth. Substrate oxide desorption was performed at ~680 °C under a constant As_2 flux and was monitored *in-situ* using reflected high energy electron diffraction (RHEED). The Ga beam equivalent pressure was kept at 2.76×10^{-7} Torr for each run, corresponding to a growth rate of ~0.5 μm/h based on RHEED intensity oscillation. For each structure, several layers of $GaAs_{1-y}Sb_y$ were grown using different As/Ga (5 to 15) and Sb/Ga (1 to 6.16) ratios as well as different substrate temperatures (375 °C-450 °C). In order to accommodate the lattice mismatch between the top $GaAs_{1-y}Sb_y$ layer and the GaAs substrate and to reduce the threading dislocation density in the final $GaAs_{1-y}Sb_y$ layer of interest, a two step-graded GaAsSb layer with different Sb compositions was incorporated in each run. The thickness of each layer was fixed at 750 nm. The growth parameters used for the different $GaAs_{1-y}Sb_y$ layers are summarized in Table I. All temperatures denoted in this study are referred to the thermocouple temperature. The alloy composition and strain relaxation properties of each $GaAs_{1-y}Sb_y$ layer were characterized by high-resolution XRD. Both the rocking curve ($\omega/2\theta$ scan) and reciprocal space maps (RSMs) of each sample surface were obtained using a Panalytical X'pert Pro system with Cu Kα-1 as the x-ray source. The structural and interface quality, as well as the defect properties, of the $GaAs_{1-y}Sb_y$ step-graded buffers were examined using transmission electron microscopy (TEM) analysis performed on a Philips EM420 microscope. The electron-transparent foils of thin-film cross-sections of $GaAs_{1-y}Sb_y$/GaAs were prepared using standard mechanical polishing techniques followed by low-temperature Ar^+ ion milling.

Following the MBE growth of the $GaAs_{1-y}Sb_y$ structures, 1.5 nm and 10 nm Al_2O_3, HfO_2, and Ta_2O_5 were deposited by ALD in a Cambridge NanoTech system using H_2O as the oxygen source and the following precursors: (i) Trimethlyaluminum (98%, Strem Chemicals), (ii) Tetrakis(dimethylamino)hafnium (99.99%, Strem Chemicals), and (iii) Tantalum(V) ethoxide

TABLE I. Summary of the growth parameters and structural analysis of the $GaAs_{1-y}Sb_y$ materials presented in this study.

	Growth parameters			Structural properties						
					Lattice constants (Å)[a]					
Run NO.	Sb/Ga	As/Ga	Growth temperature (°C)	Sb%	c	a	a_r	Relaxation (%)	FWHM (arcsec)	*rms*[b] (nm)
A	1	15	450	15	5.72	5.71	5.71	93%	188.13	1.31
	1	10	450	19	5.74	5.73	5.73	93%	90.50	
	1	5	450	21	5.75	5.73	5.74	85%	70.45	
B	2	15	450	32	5.79	5.79	5.79	97%	263.52	1.18
	2	10	450	40	5.83	5.82	5.83	97%	184.86	
	2	10	410	44	5.85	5.84	5.84	97%	132.66	
C	3	15	450	36	5.82	5.79	5.80	92%	377.60	1.85
	3	10	450	42	5.85	5.81	5.83	91%	744.33	
	3	10	410	46	5.87	5.83	5.85	91%	104.25	
D[c]	3.58	10	410	49	5.88	5.85	5.86	93%	384.58	1.73
	3.58	10	400							
	3.58	10	390							
	3.58	10	375	51	5.89	5.85	5.87	91%	729.46	
E	4.31	15	450	41	5.84	5.82	5.83	94%	443.23	1.40
	4.31	10	450	52	5.88	5.87	5.87	96%	349.20	
	4.31	10	410	57	5.91	5.88	5.90	95%	230.94	
F	6.16	15	450	44	5.85	5.84	5.84	97%	479.98	1.28
	6.16	10	450	59	5.91	5.91	5.91	99%	277.92	
	6.16	10	410	62	5.93	5.91	5.92	97%	283.71	

[a]c is the out-of-plane lattice constant, a is the in-plane constant, and a_r is the relaxed lattice constant.
[b]The surface roughness is taken from the top layer of each sample.
[c]The XRD peaks were merged together for the first three layers in sample D.

TABLE II. Summary of the deposition conditions as well as the corresponding number of growth cycles required to deposit each 1.5 nm and 10 nm thick high-κ dielectric.

Materials	GaAsSb/GaAs substrate temperature (°C)	Precursor temperature (°C)	Growth rate (Å/cycle)	Growth cycles ($t_{ox} \approx 1.5$ nm)	Growth cycles ($t_{ox} \approx 10$ nm)
Al_2O_3	250	25	1.05	15	95
HfO_2	200	75	1.01	15	100
Ta_2O_5	250	160	0.61	25	165

(99.99%, Strem Chemicals). Prior to loading each GaAsSb sample into the ALD chamber, native oxides from each $GaAs_{1-y}Sb_y$ surface were removed by 1:10 dilute hydrochloric acid. For the Al_2O_3 and Ta_2O_5 depositions, the substrate temperature was held at a constant 250 °C, while for the HfO_2 depositions, the substrate temperature was held at a constant 200 °C. To ensure that the precursor flux was sufficient to saturate each sample surface, the Hf and Ta precursors were heated to 75 °C and 160 °C, respectively, while the Al precursor was kept at room temperature. Under the aforementioned conditions, the growth rates for each Al_2O_3, Ta_2O_5, and HfO_2 oxide film were 1.05Å/cycle, 0.61Å/cycle, and 1.01Å/cycle, respectively. Table II summarizes the deposition conditions as well as the corresponding number of growth cycles required to deposit each 1.5 nm and 10 nm dielectric layer.

III. RESULTS AND DISCUSSION

A. Strain relaxation properties of $GaAs_{1-y}Sb_y$ metamorphic structures

The symmetric (004) XRD rocking curves of structures A-F are shown in Fig. 1 with the measured Sb compositions labeled together with their corresponding peaks. It can be seen from Fig. 1 that with fine-tuning of the As/Ga ratio, the Sb/Ga ratio, and the substrate temperature, the Sb composition can be precisely controlled over a wide range lying between 15% and 62%, depending on the application and the device-specific requirements. It has been reported that $GaAs_{1-y}Sb_y$ with a low Sb composition (~15%) can be used as a buffer layer to reduce dislocations in GaAs on Si multi-junction solar cell applications;[22] $GaAs_{1-y}Sb_y$ with 25% Sb has been used as a metamorphic buffer layer on GaAs substrates for 1.55 μm InAs quantum dot (QD) laser applications;[8,9] $GaAs_{1-y}Sb_y$ with 35% Sb has been used as an active layer material for resonant-cavity-enhanced p-i-n photodiode detectors;[6] $GaAs_{1-y}Sb_y$ with 50% Sb, which is lattice matched to InP, has been utilized for TFET applications;[23] and $GaAs_{1-y}Sb_y$ with an even higher Sb composition (>60%) has been reported in a mixed As/Sb-based InGaAs/GaAsSb heterostructure as a way to further improve the device performance for both n-type and p-type TFETs.[1–4] In a mixed As/Sb-based InGaAs/GaAsSb TFET structure, $GaAs_{1-y}Sb_y$ materials having a high Sb composition (>60%) are desirable for reducing the tunneling distance from the source to the channel.[3]

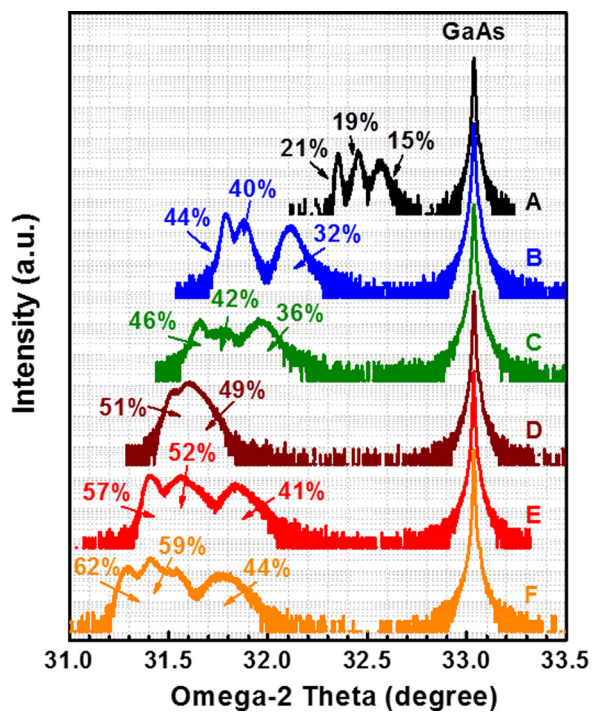

FIG. 1. Symmetric (004) XRD rocking curves of structures A-F. The measured Sb composition of each layer in each structure was also labeled to the corresponding peak.

The detailed strain relaxation state of each $GaAs_{1-y}Sb_y$ layer within each structure was analyzed from symmetric (004) and asymmetric (115) RSMs. Figures 2(a) and 2(b) show the symmetric (004) and asymmetric (115) RSMs from each $GaAs_{1-y}Sb_y$ structure, respectively. Distinct reciprocal lattice points (RLPs) were found in the RSMs of each structure, corresponding to $GaAs_{1-y}Sb_y$ materials with different Sb compositions. From the measured RSMs, the out-of-plane lattice constant, c (from the symmetric 004 reflection), and the lattice constant in the growth plane, a (from the asymmetric 115 reflection), were determined. The relaxed lattice constant, a_r, and strain relaxation values were extracted from each RSM using the methods introduced in Ref. 1. It should be noted that the extraction of strain relaxation values was performed as a sequence from the bottom layer to the top layer, and all relaxation values are determined with respect to the GaAs substrate. Table I summarizes the in-plane and out-of-plane lattice constants, relaxed layer lattice constants, and alloy composition in each layer of the different $GaAs_{1-y}Sb_y$ structures. Using the extracted alloy compositions, it can be seen that the Sb composition has a direct dependence on the As/Ga ratio, the Sb/Ga ratio, and the substrate temperature. First, the Sb composition increases with reducing growth temperature. This behavior has been attributed to an As/Sb exchange reaction that increases with increasing temperature.[13] A similar changing trend of Sb composition with temperature has also been reported by other researchers.[13,24] Second, the Sb composition increases

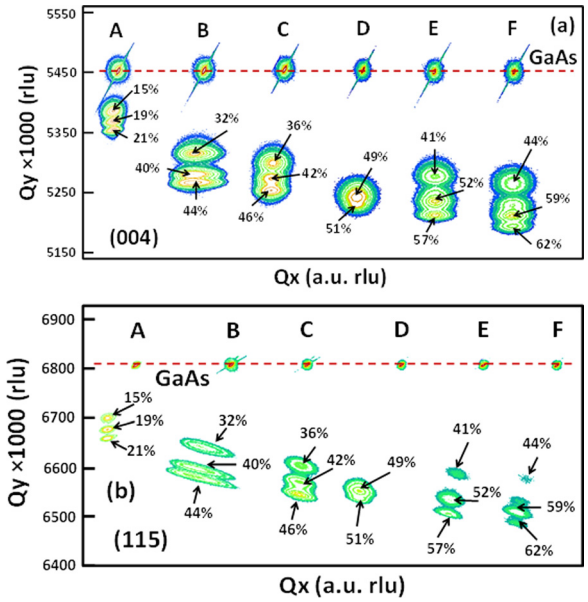

FIG. 2. (a) Symmetric (004) and (b) asymmetric (115) RSMs of samples A-F. The measured Sb composition was labeled to each reciprocal lattice point.

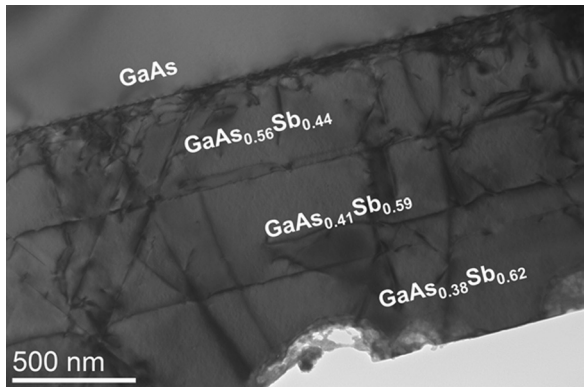

FIG. 3. Cross-sectional TEM micrograph of the mixed-anion $GaAs_{1-y}Sb_y$ structure having stepped Sb compositions of 44%, 59%, and 62% (sample F). Threading dislocations and micro-twins are shown propagating through the structure, arising from the large lattice mismatch at the $GaAs_{0.56}Sb_{0.44}$/GaAs bottom interface. Sharp heterointerfaces are observed between each $GaAs_{1-y}Sb_y$ stepped-composition epilayer. Ar^+ ion milling-induced damage was found distributed across the $GaAs_{0.38}Sb_{0.62}$ "virtual substrate" surface.

at higher Sb/Ga ratios, as expected, but appears to follow a nonlinear relationship. By comparing the first layer of samples A and B, and C and F, it can be found that at a set growth temperature of 450 °C and As/Ga ratio of 15, the Sb composition was doubled from 15% to 32% between samples A and B solely by doubling the Sb/Ga ratio from 1 to 2; however, the Sb composition only increased by 8% from 36% to 44% between samples C and F when doubling the Sb/Ga ratio from 3 to 6.16. This behavior was also reported by Wu *et al.*,[25] where the Sb content at a fixed growth temperature was found to be sensitive to change in Sb flux during growth for low Sb flux, while being less sensitive at higher Sb fluxes. Third, the reduction of the As/Ga ratio at a fixed Sb/Ga ratio and growth temperature also results in an increase in Sb composition. This is also due to the competition between the As and Sb atoms at the surface of the GaAsSb layer. The increase in Sb composition caused by the reduction of the As/Ga ratio is more sensitive at higher Sb fluxes due to the much higher incorporation efficiency of Sb over As.[5] Furthermore, it has been reported that the Sb mole fraction increases with increasing Ga fluxes when both the As and Sb fluxes as well as the growth temperature were kept constant.[5] This implies that the surface dissociation of Sb-containing species is more effective in the presence of a higher concentration of Ga flux on the surface. Thus, our results are in agreement with the prediction from non-equilibrium thermodynamical analysis for III-V-V' compounds.[26]

To gain further insight into the defect properties and structural quality of the mixed-anion $GaAs_{1-y}Sb_y$ material systems, cross-sectional TEM micrographs were taken for a Sb composition of 62% (sample F), shown in Figure 3. As shown in Fig. 3, a large fraction of misfit-induced defects resulting from the lattice mismatch between the first Sb composition layer, $GaAs_{0.56}Sb_{0.44}$ and the GaAs substrate, were confined within 0.4 μm of the $GaAs_{0.56}Sb_{0.44}$/GaAs interface. One can also observe that a large number of threading dislocations and micro-twins were found in this structure. As a result of the increased defect density, a simultaneous broadening and weakening of the $GaAs_{1-y}Sb_y$ epilayer (sample F) XRD peak intensity were found with increasing Sb compositions. Despite the high defect density, a sharp heterointerface was observed in each $GaAs_{1-y}Sb_y$ heterointerfaces, which is essential in minimizing interface and surface-related scattering in $GaAs_{1-y}Sb_y$ active layer. This also preserve and maintain staggered band alignment for a mixed As/Sb-based TFET structure.[1–4]

The surface morphology and root-mean-square (*rms*) roughness of each structure was characterized by atomic force microscopy (AFM) in contact mode using 20 μm × 20 μm surface scans. All samples exhibit a smooth surface with low *rms* roughness ranging from 1.18 nm (sample B) to 1.85 nm (sample D). The smooth surfaces are attributed to the Sb surfactant mediated growth of GaAsSb. The 20 μm × 20 μm and 1 μm × 1 μm AFM micrographs of sample F are shown in Figs. 4(a) and 4(b), respectively. Line profiles were taken in the two orthogonal ⟨110⟩ directions, shown in Fig. 4(c), which show a low peak-to-valley height of 6 nm. Mounds with several hundred nanometer dimensions appear on the high Sb composition $GaAs_{0.38}Sb_{0.62}$ surface, corresponding to a saturation region of strain relaxation.[27,28] According to Rodriguez *et al.*,[27] the strain relaxation of $GaAs_{1-y}Sb_y$ on GaAs revealed several regions which correlated to the surface morphology and the nucleation of dislocations. The fast relaxation regime is characterized by the nucleation of small islands and an abrupt increase in the number of edge dislocations, while the saturation regime is distinguished by coalesce of small islands.[27] Further, as shown in Fig. 4(a), a two-dimensional (2D) surface network in the [110] and [1$\bar{1}$0] directions can be found on the surface of structure F. This surface morphology corresponds to the strain relaxation properties of the graded buffer layers. The graded buffer primarily relaxes lattice mismatch by the formation of 60° a/2 ⟨110⟩ {111} misfit dislocations at the epilayer/substrate interface and the interfaces between different steps. These dislocations can glide along {111} planes and

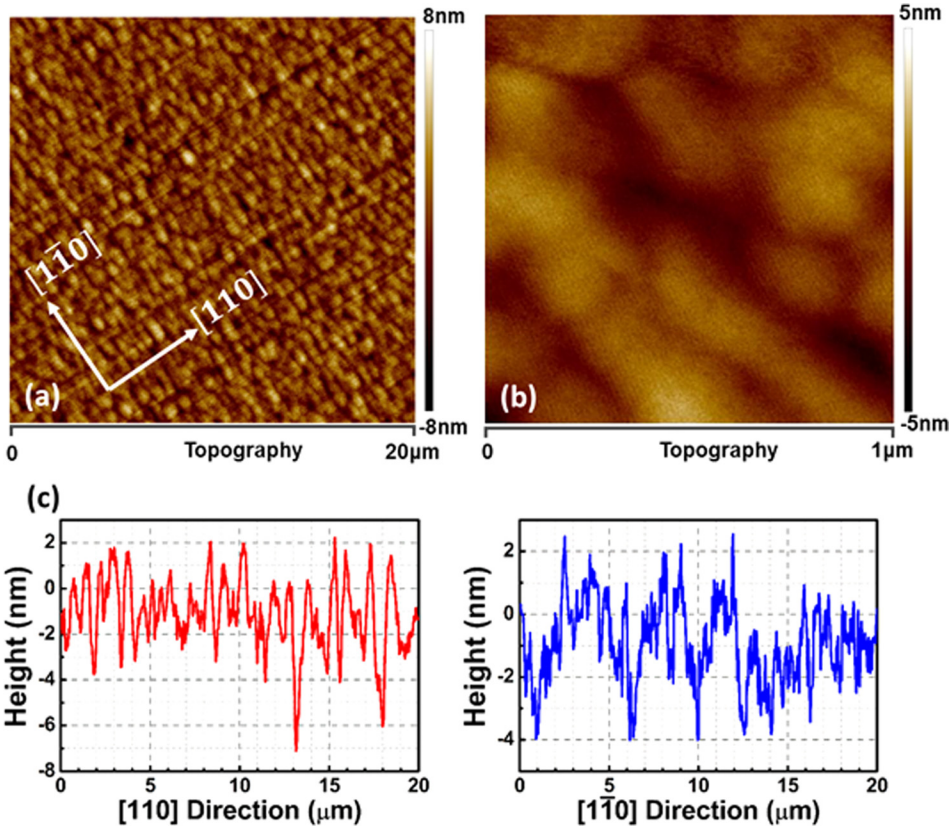

FIG. 4. AFM micrographs of sample F ($GaAs_{0.38}Sb_{0.62}$) from (a) a 20 μm × 20 μm scan and (b) a 1 μm × 1 μm scan. The *rms* roughness was determined to be 1.28 nm from the 20 μm × 20 μm scan. Mounds with dimensions of several hundred nanometers appear on the 1 μm × 1 μm scan, corresponding to a saturation region of strain relaxation. Line profiles along the two orthogonal ⟨110⟩ directions taken from the 20 μm × 20 μm scan are shown by (c).

thread towards the surface at a 60° angle within ⟨110⟩ directions, which results in a cross-hatch pattern on the sample surface.[1–5] Lubyshev *et al.*[29] reported similar surface morphology using a graded $GaAs_{1-y}Sb_y$ buffer. A combination of mound-like features and a 2D surface network correspond to the nucleation of the $GaAs_{1-y}Sb_y$ layer and the graded composition in multiple $GaAs_{1-y}Sb_y$ buffer layers, respectively.[29] Furthermore, both Lubyshev *et al.*[29] and Wang *et al.*[30] reported a nearly fully relaxed strain state of $GaAs_{1-y}Sb_y$ graded buffers, indicating that the $GaAs_{1-y}Sb_y$ buffer effectively accommodates the lattice mismatch between the active layers and the substrate. Structures A-E show similar surface morphology (not shown here) as structure F, indicating identical strain relaxation characteristics of $GaAs_{1-y}Sb_y$ layers having different Sb compositions. The saturation of strain relaxation also agrees with the strain relaxation analysis as summarized in Table I.

B. High-κ dielectric integration and band offset determination on $GaAs_{0.38}Sb_{0.62}$

$GaAs_{1-y}Sb_y$ materials with high Sb compositions (>60%) have great potential for future TFET applications.[1–4] It has been reported that the device performance has been improved significantly by utilizing a $GaAs_{0.35}Sb_{0.65}$ layer in n-channel $In_{0.7}Ga_{0.3}As/GaAs_{0.35}Sb_{0.65}$ staggered gap TFET structures when compared with $In_{0.7}Ga_{0.3}As$ homojunction TFET device structures.[23,31] Meanwhile, it is equally important to develop high-performance p-type TFET devices within the same material system to enable complementary energy efficient logic circuits.[32] In a p-type TFET structure, n^{++} $In_xGa_{1-x}As$ material is used as the source and undoped $GaAs_{1-y}Sb_y$ material is used as the channel,[3,32] where the dielectric material is integrated onto the high Sb composition $GaAs_{1-y}Sb_y$ channel material in order to lower the tunneling barrier height and increase the tunneling probability. In this regard, key considerations for selecting high-κ dielectric materials on $GaAs_{1-y}Sb_y$ active channel layer are the valence band and conduction band offsets >1 eV in order to minimize the carrier injection from the semiconductor into the insulator.[21] As a result, the integration of different high-κ dielectrics on $GaAs_{1-y}Sb_y$ (y > 60%) as well as an understanding of the interfacial properties are vital for advancing further development of TFET devices for low-power implantable devices. Moreover, the research of different high-κ dielectric materials on $GaAs_{1-y}Sb_y$ can also provide information for future studies on the utilization and suitability of $GaAs_{1-y}Sb_y$ (y > 60%) material systems in multifunctional device applications. In practice, Al_2O_3, HfO_2, and Ta_2O_5 are three commonly used high-κ dielectric materials for advanced field-effect-transistor applications due to their high dielectric constants (~9 for Al_2O_3, ~25 for HfO_2, and 20~25 for amorphous Ta_2O_5 and as high as 52 for crystalline Ta_2O_5 [33]), relatively high band gap energies, and high thermal and chemical stability. In this study, a detailed XPS analysis was conducted to determine the band offsets of Al_2O_3, HfO_2, and Ta_2O_5 on high Sb composition $GaAs_{0.38}Sb_{0.62}$ material. The valence band offset (VBO) values were measured using Kraut's method.[34] The conduction band offset (CBO) values were calculated using the measured VBO values and the band gap energies of $GaAs_{0.38}Sb_{0.62}$, Al_2O_3, HfO_2, and Ta_2O_5, respectively.

The band alignments of Al_2O_3, HfO_2, and Ta_2O_5 on $GaAs_{0.38}Sb_{0.62}$ were investigated using a PHI Quantera SXM XPS system with a monochromatic Al-Kα (energy of 1486.7eV) x-ray source. The VBO values between Al_2O_3 (HfO_2 or Ta_2O_5) and $GaAs_{0.38}Sb_{0.62}$ were determined by measuring the binding energy from shallow core levels (CLs) of Sb 4*d*, Al 2*p* (Hf 4*f*, Ta 4*f*) and the corresponding valence band maxima (VBM) from each material, respectively. The schematic diagram of the structures used in this study is shown in Fig. 5. As shown in Fig. 5, XPS spectra were collected from three samples of each high-κ dielectric material: (1) 1.5 nm Al_2O_3 (HfO_2 or Ta_2O_5)/750 nm $GaAs_{0.38}Sb_{0.62}$ was used to measure the CL binding energy of Al (Hf or Ta) and Sb at the interface; (2) 10 nm Al_2O_3 (HfO_2 or Ta_2O_5)/750 nm $GaAs_{0.38}Sb_{0.62}$ was used to measure the CL binding energy of Al (Hf or Ta) and VBM of Al_2O_3 (HfO_2 or Ta_2O_5); (3) 750 nm $GaAs_{0.38}Sb_{0.62}$ without the top dielectric layer was used to measure the CL binding energy of Sb and VBM of $GaAs_{0.38}Sb_{0.62}$. Sample charging occurred during the XPS measurements and was particularly problematic on the fully oxidized materials.[21] Compensation of the charging by an electron flood source was used in all measurements in order to minimize the binding energy shift. Additionally, the measured CLs and VBM binding energy values were corrected by shifting the measured carbon 1s CL peak to 285.0 eV. All XPS spectra were recorded using a pass energy of 26 eV and a step size of 0.025 eV. Curve fitting was performed with CasaXPS 2.3.14 using a Lorentzian convolution with a Shirley-type background.

After collecting the binding energy information from each sample surface, the VBO value can be determined by Kraut's method[34]

$$\Delta E_V = (E_{CL}^{GaAsSb} - E_{VBM}^{GaAsSb}) - (E_{CL}^{Oxide} - E_{VBM}^{Oxide}) + \Delta E_{CL}(i), \quad (1)$$

where E_{CL}^{GaAsSb} and E_{CL}^{Oxide} are shallow CL binding energies of Sb 4*d* and Al 2*p* (Hf 4*f* or Ta 4*f*), respectively. E_{VBM}^{GaAsSb} and E_{VBM}^{Oxide} are the VBM of $GaAs_{0.38}Sb_{0.62}$ and Al_2O_3 (HfO_2 or Ta_2O_5), respectively. E_{VBM} of each material was determined by linearly fitting the leading edge of the valence band spectra to the base line.[2,3,21] $\Delta E_{CL}(i) = E_{CL}^{Oxide}(i) - E_{CL}^{GaAsSb}(i)$ is the CL binding energy difference between Al 2*p* (Hf 4*f* or Ta 4*f*) and Sb 4*d* measured at the interface of 1.5 nm Al_2O_3 (HfO_2 or Ta_2O_5)/750 nm $GaAs_{0.38}Sb_{0.62}$ for each structure. Once the VBO was obtained, the conduction band offset (CBO) can be estimated by[2,3,21]

$$\Delta E_C = E_G^{Oxide} - \Delta E_V - E_G^{GaAsSb}, \quad (2)$$

where E_G^{Oxide} and E_G^{GaAsSb} are the band gap energies of Al_2O_3 (HfO_2 or Ta_2O_5) and $GaAs_{0.38}Sb_{0.62}$, respectively. The band gap energy of Al_2O_3, HfO_2, and Ta_2O_5 were found to be 6.50 eV,[35] 5.52 eV (Ref. 36) and 4.40 eV.[37] The band gap energy of $GaAs_{0.38}Sb_{0.62}$ is determined to be 0.7 eV by empirical modeling.[38]

Figure 6(a) shows the Sb 4*d* CL and $GaAs_{0.38}Sb_{0.62}$ VB spectra from the surface of the 750 nm $GaAs_{0.38}Sb_{0.62}$ layer. Figure 6(b) shows the Al 2*p* CL and Sb 4*d* CL spectra measured at the interface of 1.5 nm Al_2O_3/750 nm $GaAs_{0.38}Sb_{0.62}$.

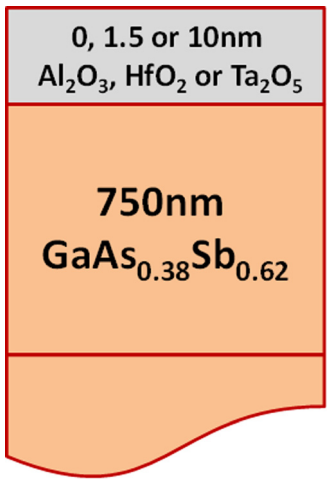

FIG. 5. Schematic diagram of the high-κ dielectric materials (Al_2O_3, HfO_2 and Ta_2O_5) integrated on $GaAs_{0.38}Sb_{0.62}$ for band alignment measurements.

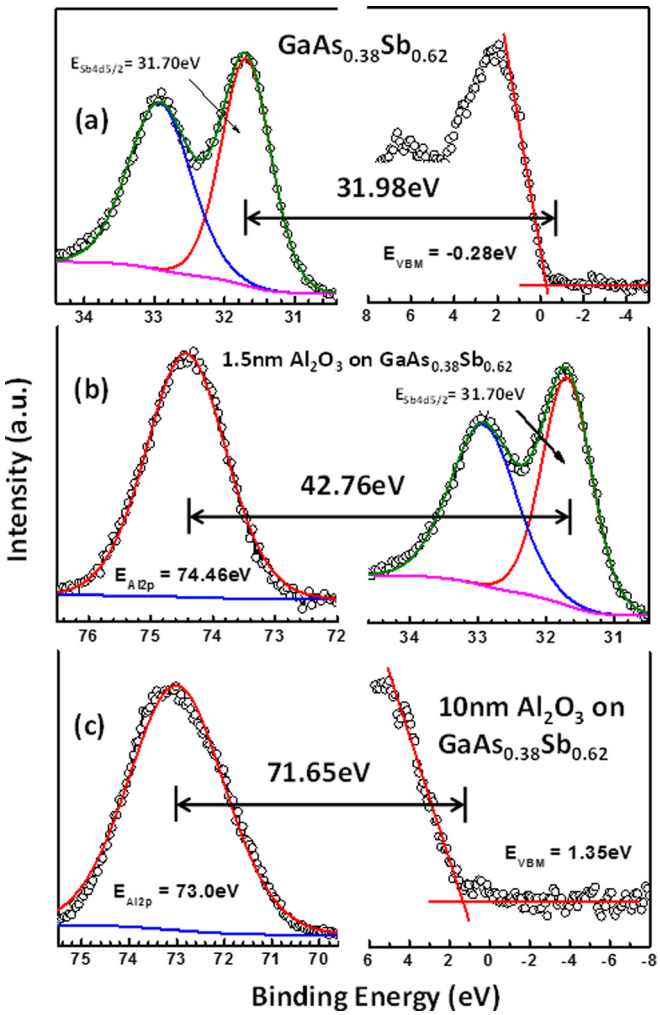

FIG. 6. XPS spectra of (a) the Sb 4*d* core level and valence band from bulk $GaAs_{0.38}Sb_{0.62}$; (b) the Al 2*p* and Sb 4*d* core levels from 1.5 nm Al_2O_3 on bulk $GaAs_{0.38}Sb_{0.62}$; (c) the Al 2*p* core level and valence band from 10 nm Al_2O_3 on bulk $GaAs_{0.38}Sb_{0.62}$. Core level spectra were fitted using a Lorentzian convolution with a Shirley-type background. The valence band maximum is determined by linearly fitting the leading edge of the valence band spectrum to the base line.

TABLE III. Summary of the core level peak positions and valence band maxima (VBM) from bulk $GaAs_{0.38}Sb_{0.62}$, Al_2O_3, HfO_2 and Ta_2O_5 on $GaAs_{0.38}Sb_{0.62}$.

Structures	Peak assignment	Binding energy (eV)	Band offset[a]
750 nm $GaAs_{0.38}Sb_{0.62}$	Sb4d5/2	31.70	
	VBM	−0.28	
1.5 nm Al_2O_3 on $GaAs_{0.38}Sb_{0.62}$	Al2p	74.46	$\Delta E_C = 2.71$ eV $\Delta E_V = 3.09$ eV
	Sb4d5/2	31.70	
10 nm Al_2O_3 on $GaAs_{0.38}Sb_{0.62}$	Al2p	73.00	
	VBM	1.35	
1.5 nm HfO_2 on $GaAs_{0.38}Sb_{0.62}$	Sb4d5/2	31.80	$\Delta E_C = 2.09$ eV $\Delta E_V = 2.73$ eV
	Hf4f7/2	16.80	
10 nm HfO_2 on $GaAs_{0.38}Sb_{0.62}$	Hf4f7/2	16.55	
	VBM	2.30	
1.5 nm Ta_2O_5 on $GaAs_{0.38}Sb_{0.62}$	Sb4d5/2	31.70	$\Delta E_C = 0.71$ eV $\Delta E_V = 2.99$ eV
	Ta4f7/2	26.14	
10 nm Ta_2O_5 on $GaAs_{0.38}Sb_{0.62}$	Ta4f7/2	26.05	
	VBM	2.62	

[a]ΔE_C is calculated using the measured value of ΔE_V and the band gap energy of $GaAs_{0.38}Sb_{0.62}$, Al_2O_3, HfO_2, and Ta_2O_5, respectively.

Figure 6(c) shows the Al 2*p* CL and Al_2O_3 VB spectra from 10 nm Al_2O_3/750 nm $GaAs_{0.38}Sb_{0.62}$. The measured and fitted peak positions from each structure are summarized in Table III. The results show that the value of $(E_{Al2p}^{Al2O3} - E_{VBM}^{Al2O3})$ is 71.65 eV. The measured value of $(E_{Sb4d5/2}^{GaAsSb} - E_{VBM}^{GaAsSb})$ is 31.98 eV. The binding energy difference between the Al 2*p* and the Sb $4d_{5/2}$ states at the interface $(\Delta E_{CL}(i))$ was found to be 42.76 eV. Using these measured values, the VBO of $GaAs_{0.38}Sb_{0.62}$ with respect to Al_2O_3 was determined to be 3.09 ± 0.05 eV. The uncertainty value of 0.05 eV results from the curve fitting process and the selection of the data points for the fitting of the VBM position. Similar measurements were also performed on $HfO_2/GaAs_{0.38}Sb_{0.62}$ and $Ta_2O_5/GaAs_{0.38}Sb_{0.62}$ structures. The CL and VB spectra from $HfO_2/GaAs_{0.38}Sb_{0.62}$ and $Ta_2O_5/GaAs_{0.38}Sb_{0.62}$ are shown in Figs. 7(a), 7(b), 8(a), and 8(b), respectively. The peak positions from the measured and fitted results are summarized in Table III. The VBO is 2.73 ± 0.05 eV for $HfO_2/GaAs_{0.38}Sb_{0.62}$ and 2.99 ± 0.05 eV for $Ta_2O_5/GaAs_{0.38}Sb_{0.62}$. The CBO values of all three high-κ dielectrics on $GaAs_{0.38}Sb_{0.62}$ are estimated from Eq. (2) using band gap energies of Al_2O_3, HfO_2, Ta_2O_5, and $GaAs_{0.38}Sb_{0.62}$ together with the measured VBO values. The CBO was calculated to be ~2.71 eV for $Al_2O_3/GaAs_{0.38}Sb_{0.62}$, ~2.09 eV for $HfO_2/GaAs_{0.38}Sb_{0.62}$ and ~0.71 eV for $Ta_2O_5/GaAs_{0.38}Sb_{0.62}$, respectively. All calculated CBO values are also summarized in Table III.

It should be noted that while the Sb 4*d* spectra for the thin $Al_2O_3/GaAs_{0.38}Sb_{0.62}$ interface is free of Sb-O bonding, indicative of a Sb native oxide-free $GaAs_{1-y}Sb_y$ surface, low and high intensity Sb-O states were observed at the thin HfO_2 and $Ta_2O_5/GaAs_{0.38}Sb_{0.62}$ interfaces, respectively. Recent reports[39] have demonstrated that a thin Ga native oxide (i.e., Ga_2O_3) aids in improving the electrical quality of the dielectric/GaSb interface, while Sb (or Ga) native oxide formation between the dielectric and GaSb (or dielectric and GaAs) interface, have been reported to be detrimental to the electrical device quality.[39,40] Recent attempts have been made to passivate the surface of GaSb (or GaAs) using *in-situ* hydrogen passivation or combination of ex-situ wet chemical passivation, e.g., $(NH_4)_2S$ along with hydrogen passivation prior to deposition of high-κ dielectrics. These passivation methods helped to improve the reduction of Sb native-oxides compared with only HCl cleaning of the Sb-based materials.[39,41,42] In fact, the interfacial oxide layer between the dielectric and the GaSb (GaAs) was reported to increase the interfacial band bending,[43] which could affect the extracted VBO and CBO. In this work, there is no significant shift in Sb 4*d* CL positions for Al_2O_3 and Ta_2O_5 interfaces with GaAsSb, even if there is a minimal amount of

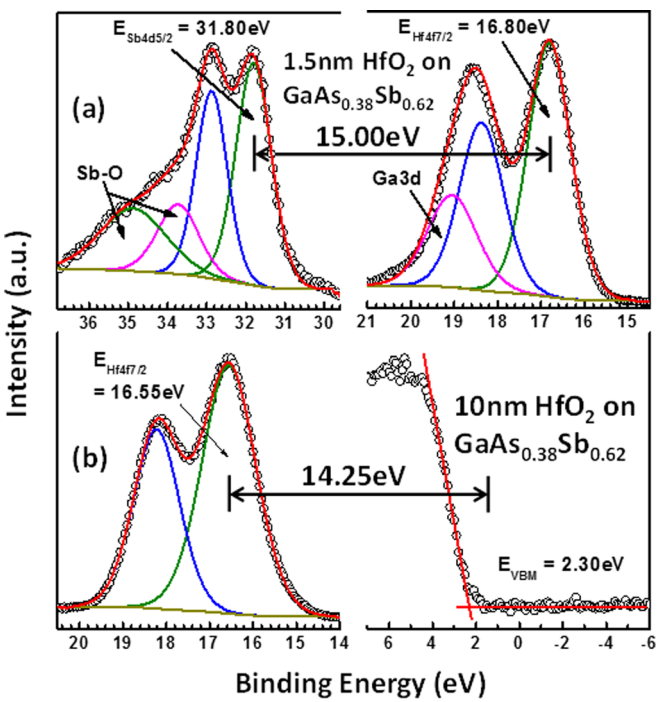

FIG. 7. XPS spectra of (a) the Sb 4*d* and Hf 4*f* core levels from 1.5 nm HfO_2 on bulk $GaAs_{0.38}Sb_{0.62}$; (b) the Hf 4*f* core level and valence band from 10 nm HfO_2 on bulk $GaAs_{0.38}Sb_{0.62}$. Core level spectra were fitted using a Lorentzian convolution with a Shirley-type background. The valence band maximum is determined by linearly fitting the leading edge of the valence band spectrum to the base line.

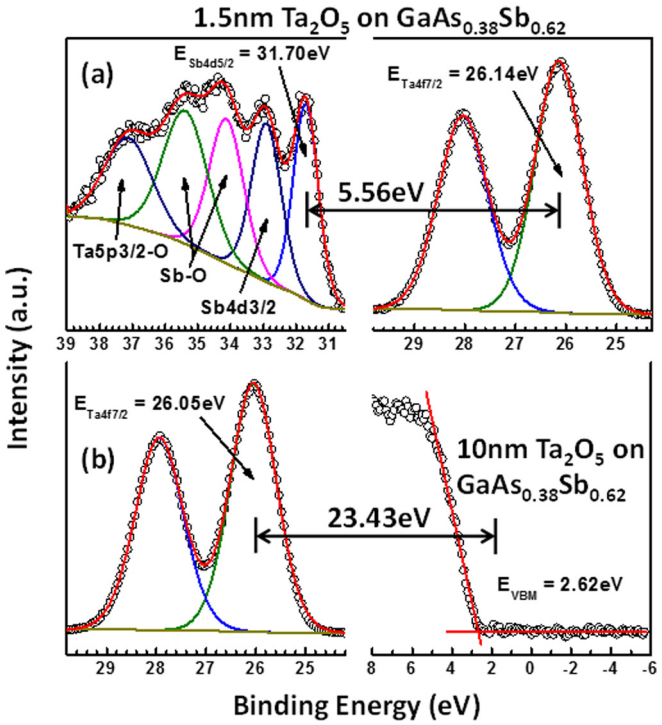

FIG. 8. XPS spectra of (a) the Sb 4*d* and Ta 4*f* core levels from 1.5 nm Ta_2O_5 on bulk $GaAs_{0.38}Sb_{0.62}$; (b) the Ta 4*f* core level and valence band from 10 nm Ta_2O_5 on bulk $GaAs_{0.38}Sb_{0.62}$. Core level spectra were fitted using a Lorentzian convolution with a Shirley-type background. The valence band maximum is determined by linearly fitting the leading edge of the valence band spectrum to the base line.

native Sb oxide formed during the ALD deposition process for Ta_2O_5 and HfO_2. On the other hand, a small shift of 0.1eV for the HfO_2/GaAsSb interface was observed, however, this shift is within the error bar of the measured band offsets.

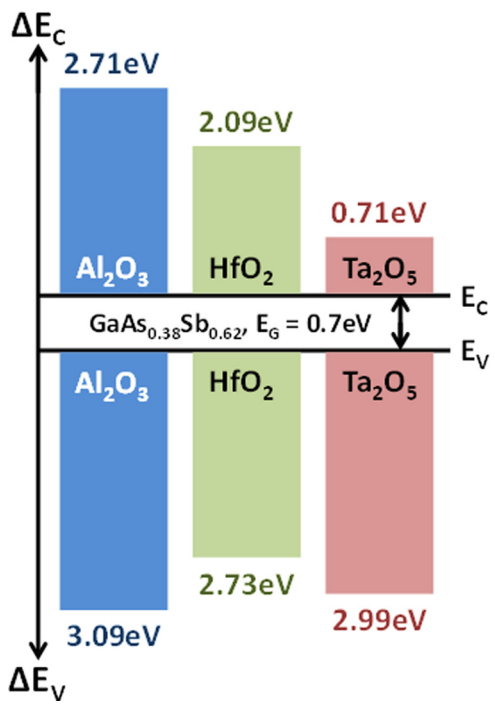

FIG. 9. Histogram of valence and conduction band offset distribution for Al_2O_3, HfO_2 and Ta_2O_5 on $GaAs_{0.38}Sb_{0.62}$.

Figure 9 shows the histogram of ΔE_V and ΔE_C distributions for Al_2O_3, HfO_2, and Ta_2O_5 on $GaAs_{0.38}Sb_{0.62}$ based on the results presented above. It can be seen from this figure that all three high-κ dielectrics provide a valence band offset on $GaAs_{0.38}Sb_{0.62}$ greater than 2 eV, which indicates that all three high-κ dielectric materials can be integrated on $GaAs_{0.38}Sb_{0.62}$ for p-type FET applications, especially for use with TFET devices.[1–3] Regarding the conduction band alignment, both Al_2O_3 and HfO_2 can provide CBO values also >2 eV, suggesting that these two oxide materials can also be used on $GaAs_{0.38}Sb_{0.62}$ for n-type FET applications. However, the CBO value of Ta_2O_5 on $GaAs_{0.38}Sb_{0.62}$ is limited to 0.71 eV due to the low band gap energy of Ta_2O_5.[33,37] As a result, additional interfacial dielectric layer could be integrated between the Ta_2O_5 and the $GaAs_{0.38}Sb_{0.62}$ in order to utilize Ta_2O_5 as part of a composite dielectric stack on $GaAs_{0.38}Sb_{0.62}$ for n-type FET applications. In addition, further investigations are needed to study the electrical transport properties of utilizing Al_2O_3, HfO_2, and Ta_2O_5 as high-κ dielectric materials on $GaAs_{0.38}Sb_{0.62}$. The measured band offset values between Al_2O_3, HfO_2, Ta_2O_5, and $GaAs_{0.38}Sb_{0.62}$ will provide a critical reference for the future design of a mixed As/Sb-based TFET structure and other multifunctional devices.

IV. CONCLUSION

Mixed-anion metamorphic $GaAs_{1-y}Sb_y$ materials with a wide range of Sb compositions were grown by solid source MBE. By optimizing the As/Ga and Sb/Ga ratios as well as the substrate temperature, the Sb composition in $GaAs_{1-y}Sb_y$ was precisely controlled in the range of 15% to 62%. X-ray diffraction analysis indicates nearly full relaxation of each $GaAs_{1-y}Sb_y$ layer. Atomic force microscopy studies revealed smooth surface morphologies across the wide range of Sb compositions. Three high-κ dielectric materials, Al_2O_3, HfO_2, and Ta_2O_5, were deposited on $GaAs_{0.38}Sb_{0.62}$ by atomic layer deposition. X-ray photoelectron spectroscopy measurements indicate a valence band offset of >2 eV for all three dielectric materials on $GaAs_{0.38}Sb_{0.62}$, suggesting the potential for utilizing these dielectrics on $GaAs_{0.38}Sb_{0.62}$ for p-type metal-oxide-semiconductor applications. Both Al_2O_3 and HfO_2 exhibit conduction band offset values of >2 eV on $GaAs_{0.38}Sb_{0.62}$, indicating that these two dielectrics can also be used for n-type MOS applications. However, Ta_2O_5 exhibits a low conduction band offset value of 0.71 eV due to its limited bandgap energy. Therefore, the precise control of Sb composition during MBE growth of $GaAs_{1-y}Sb_y$ metamorphic materials, as well as the detailed band alignment analysis of three high-κ dielectrics on $GaAs_{0.38}Sb_{0.62}$, paves the way for the future integration of $GaAs_{1-y}Sb_y$ materials in microelectronic and optoelectronic applications.

ACKNOWLEDGMENTS

This work was supported in part by the National Science Foundation under Grant No. ECCS-1028494 and Intel Corporation. P.G. acknowledges support from the National Science Foundation Graduate Research Fellowship under

Grant No. DGE 0822220. The authors would like to acknowledge NCFL-Institute for Critical Technology and Applied Sciences (ICTAS) and Virginia Tech Nanofabrication Facilities for materials characterization.

[1]Y. Zhu, N. Jain, S. Vijayaraghavan, D. K. Mohata, S. Datta, D. Lubyshev, J. M. Fastenau, W. K. Liu, N. Monsegue, and M. K. Hudait, J. Appl. Phys. **112**, 024306 (2012).
[2]Y. Zhu, N. Jain, D. K. Mohata, S. Datta, D. Lubyshev, J. M. Fastenau, A. K. Liu, and M. K. Hudait, Appl. Phys. Lett. **101**, 112106 (2012).
[3]Y. Zhu and M. K. Hudait, Nanotechnol. Rev. **2**, 637 (2013).
[4]B. Rajamohanan, D. Mohata, Y. Zhu, M. Hudait, Z. Jiang, M. Hollander, G. Klimeck, and S. Datta, J. Appl. Phys. **115**, 044502 (2014).
[5]A. Bosacchi, S. Franchi, P. Allegri, V. Avanzini, A. Baraldi, R. Magnanini, M. Berti, D. De Salvador, and S. K. Sinha, J. Cryst. Growth **201–202**, 858 (1999).
[6]S. Xiaoguang, W. Shuling, J. S. Hsu, R. Sidhu, X. G. Zheng, X. Li, J. C. Campbell, and A. L. Holmes, IEEE J. Sel. Topics Quantum Electron. **8**, 817 (2002).
[7]H. Shimizu and S. Saravanan, Appl. Phys. Lett. **88**, 041119 (2006).
[8]Y. Qiu, T. Walther, H. Y. Liu, C. Y. Jin, M. Hopkinson, and A. G. Cullis, in *Microscopy of Semiconducting Materials 2007*, edited by A. G. Cullis and P. A. Midgley (Springer, Netherlands, 2008), Vol. 120, pp. 263-268.
[9]H. Y. Liu, Y. Qiu, C. Y. Jin, T. Walther, and A. G. Cullis, Appl. Phys. Lett. **92**, 111906 (2008).
[10]Y. G. Sadofyev, N. Samal, B. A. Andreev, V. I. Gavrilenko, S. V. Morozov, A. G. Spivakov, and A. N. Yablonsky, Semiconductors **44**, 405 (2010).
[11]J. R. Pessetto and G. B. Stringfellow, J. Cryst. Growth **62**, 1 (1983).
[12]T. Waho, S. Ogawa, and S. Maruyama, Jpn J. Appl. Phys., Part 1 **16**, 1875 (1977).
[13]S. P. Bremner, G. M. Liu, N. Faleev, K. Ghosh, and C. B. Honsberg, J. Vac. Sci. Technol. B **26**, 1149 (2008).
[14]B. Rajamohanan, D. Mohata, D. Zhernokletov, B. Brennan, R. M. Wallace, R. Engel-Herbert, and S. Datta, Appl. Phys. Express **6**, 101201 (2013).
[15]B. Brennan, D. M. Zhernokletov, H. Dong, C. L. Hinkle, J. Kim, and R. M. Wallace, Appl. Phys. Lett. **100**, 151603 (2012).
[16]Y. Hwang, V. Chobpattana, J. Y. Zhang, J. M. LeBeau, R. Engel-Herbert, and S. Stemmer, Appl. Phys. Lett. **98**, 142901 (2011).
[17]V. Chobpattana, J. Son, J. J. M. Law, R. Engel-Herbert, C.-Y. Huang, and S. Stemmer, Appl. Phys. Lett. **102**, 022907 (2013).
[18]A. Ali, H. S. Madan, A. P. Kirk, D. A. Zhao, D. A. Mourey, M. K. Hudait, R. M. Wallace, T. N. Jackson, B. R. Bennett, J. B. Boos, and S. Datta, Appl. Phys. Lett. **97**, 143502 (2010).
[19]A. Nainani, Y. Sun, T. Irisawa, Z. Yuan, M. Kobayashi, P. Pianetta, B. R. Bennett, J. Brad Boos, and K. C. Saraswat, J. Appl. Phys. **109**, 114908 (2011).
[20]K. Suzuki, Y. Harada, F. Maeda, K. Onomitsu, T. Yamaguchi, and K. Muraki, Appl. Phys. Express **4**, 125702 (2011).
[21]Y. Zhu, N. Jain, M. K. Hudait, D. Maurya, R. Varghese, and S. Priya, J. Vac. Sci. Technol. B **32**, 011217 (2014).
[22]O. Morohara, H. Geka, Y. Moriyasu, and N. Kuze, in *40th IEEE Photovoltaic Specialists Conference* (2014).
[23]D. K. Mohata, R. Bijesh, S. Mujumdar, C. Eaton, R. Engel-Herbert, T. Mayer, V. Narayanan, J. M. Fastenau, D. Loubychev, A. K. Liu, and S. Datta, in *IEEE Conference of Electron Devices Meeting (IEDM)* (2011), p. 781.
[24]E. Selvig, B. O. Fimland, T. Skauli, and R. Haakenaasen, J. Cryst. Growth **227–228**, 562 (2001).
[25]S. D. Wu, L. W. Guo, W. X. Wang, Z. H. Li, X. Z. Shang, H. Y. Hu, Q. Huang, and J. M. Zhou, J. Cryst. Growth **270**, 359 (2004).
[26]A. Y. Egorov, A. R. Kovsh, V. M. Ustinov, A. E. Zhukov, P. S. Kop'ev, and C. W. Tu, J. Cryst. Growth **188**, 69 (1998).
[27]B. P. Rodriguez and J. M. Millunchick, J. Appl. Phys. **100**, 044503 (2006).
[28]J. Wang, G.-W. Wang, Y.-Q. Xu, J.-L. Xing, W. Xiang, B. Tang, Y. Zhu, Z.-W. Ren, Z.-H. He, and Z. C. Niu, J. Appl. Phys. **114**, 013704 (2013).
[29]D. Lubyshev, J. M. Fastenau, Y. Qiu, A. W. K. Liu, E. J. Koerperick, J. T. Olesberg, D. Norton, N. N. Faleev, and C. B. Honsberg, Proc. SPIE **8704**, 870412 (2013).
[30]D. Wang, Y. Lin, D. Donetsky, G. Kipshidze, L. Shterengas, G. Belenky, S. P. Svensson, W. L. Sarney, and H. Hier, Proc. SPIE **8704**, 870410 (2013).
[31]D. K. Mohata, R. Bijesh, Y. Zhu, M. K. Hudait, R. Southwick, Z. Chbili, D. Gundlach, J. Suehle, J. M. Fastenau, D. Loubychev, A. K. Liu, T. S. Mayer, V. Narayanan, and S. Datta, in *IEEE Conference Symposia on VLSI Technology* (2012), p. 53.
[32]Y. Zhu, M. K. Hudait, D. K. Mohata, B. Rajamohanan, S. Datta, D. Lubyshev, J. M. Fastenau, and A. K. Liu, J. Vac. Sci. Technol. B **31**, 041203 (2013).
[33]J. Robertson, Eur. Phys. J Appl. Phys. **28**, 265 (2004).
[34]E. A. Kraut, R. W. Grant, J. R. Waldrop, and S. P. Kowalczyk, Phys. Rev. Lett. **44**, 1620 (1980).
[35]M. K. Hudait, Y. Zhu, D. Maurya, S. Priya, P. K. Patra, A. W. K. Ma, A. Aphale, and I. Macwan, J. Appl. Phys. **113**, 134311 (2013).
[36]M. K. Hudait and Y. Zhu, J. Appl. Phys. **113**, 114303 (2013).
[37]J. Robertson, J. Vac. Sci. Technol. B **18**, 1785 (2000).
[38]T. S. Wang, J. T. Tsai, K. I. Lin, J. S. Hwang, H. H. Lin, and L. C. Chou, Mater. Sci. Eng. B **147**, 131 (2008).
[39]L. B. Ruppalt, E. R. Cleveland, J. G. Champlain, S. M. Prokes, J. B. Boos, D. Park, and B. R. Bennett, Appl. Phys. Lett. **101**, 231601 (2012).
[40]N. V. Nguyen, O. A. Kirillov, W. Jiang, W. Wang, J. S. Suehle, P. D. Ye, Y. Xuan, N. Goel, K.-W. Choi, W. Tsai, and S. Sayan, Appl. Phys. Lett. **93**, 082105 (2008).
[41]D. M. Zhernokletov, H. Dong, B. Brennan, M. Yakimov, V. Tokranov, S. Oktyabrsky, J. Kim, and R. M. Wallace, Appl. Phys. Lett. **102**, 131602 (2013).
[42]V. B. Bermudez, J. Appl. Phys. **114**, 024903 (2013).
[43]F. S. Aguirre-Tostado, M. Milojevic, K. J. Choi, H. C. Kim, C. L. Hinkle, E. M. Vogel, J. Kim, T. Yang, Y. Xuan, P. D. Ye, and R. M. Wallace, Appl. Phys. Lett. **93**, 061907 (2008).